Available online at www.sciencedirect.com
SCIENCE DIRECT
Polymer 46 (2005) 9064–9080
polymer
www.elsevier.com/locate/polymer

A model for composites containing three-dimensional ellipsoidal inclusions

K.Y. Lee[a], D.R. Paul[b,*]

[a]Department of Polymer Science and Engineering, Chungnam National University, Daejeon, South Korea
[b]Department of Chemical Engineering, Texas Materials Institute, University of Texas at Austin, Austin, TX 78712, USA

Received 2 March 2005; accepted 29 June 2005
Available online 10 August 2005

Abstract

A model is developed for the mechanical properties of composites containing complex inclusions with no axes of symmetry, e.g. three dimensional ellipsoids ($a_1 > a_2 > a_3$) characterized by two aspect ratios, $\alpha = a_1/a_3$ and $\beta = a_1/a_2$, by using the Eshelby's equivalent tensor with a Mori–Tanaka type model.

The influences of the primary and secondary aspect ratios on the effective elastic moduli of nanocomposites containing aligned isotropic inclusions are examined. The model is limited to unidirectionally aligned inclusions where both the matrix and the inclusions have linearly elastic, homogeneous properties. The longitudinal moduli (E_{11}, E_{22} and E_{33}) and the shear moduli (μ_{12}, μ_{13} and μ_{23}) are calculated. The longitudinal Young's modulus E_{11} increases, as the primary and secondary aspect ratios increase. However, the transverse Young's modulus E_{22} and shear modulus μ_{12} decrease, as the secondary aspect ratio increases.

Keywords: Composites; Eshelby tensor; Ellipsoids

1. Introduction

Composite materials are usually designed to offer the advantage of high strength and stiffness with light weight. Many types of reinforced plastics customized for general purpose uses or high-technical applications have appeared in recent years. The mechanical properties are widely varied by the combinations of the kind of polymer matrix and filler used, such as polypropylene and glass fiber, epoxy resin and carbon fiber, polyamide and organoclay, etc. For efficient design and formulation of composites, it is important to have appropriate theories for the prediction of mechanical properties, thermal expansion, and other behavior in terms of the elastic properties of the matrix and filler, the geometry of the filler particles (or inclusions), and the overall morphology of the composite.

The various theories for composites usually regard the filler particles as spherical, cylindrical, or disc shaped, and analyze their contributions to properties using the solution for 2-dimensional problems. In some composites, like nanocomposites based on exfoliated aluminosilicate platelets from montmorillonite-based organoclays, the particle shape may be more complex. It would be of interest to develop theories for composites that appropriately deal with complex inclusions with no axes of symmetry and that are possibly irregular in shape. Composites based on such particles can have properties that are different in all three coordinate directions and critically dependent on the alignment achieved during processing.

Our interest in such problems was stimulated by observations on nanocomposites formed by exfoliation of aluminosilicate platelets of montmorillonite-based organoclays in a polyamide matrix. The transmission electron microscopy images taken along the flow, transverse and normal directions of injection-molded specimens in the report by Yoon and et al. [1] reveal particles with a complex distribution of shapes; an example is shown in Fig. 1. Using AFM, direct observations for the individual platy montmorillonite particles were reported by Yalcin and Cakmak [2]. These examples clearly indicate that the particles in the

* Corresponding author. Tel.: +1 512 471 5392; fax: +1 512 471 0542.
E-mail address: drp@che.utexas.edu (D.R. Paul).

0032-3861/$ - see front matter © 2005 Elsevier Ltd. All rights reserved.
doi:10.1016/j.polymer.2005.06.113

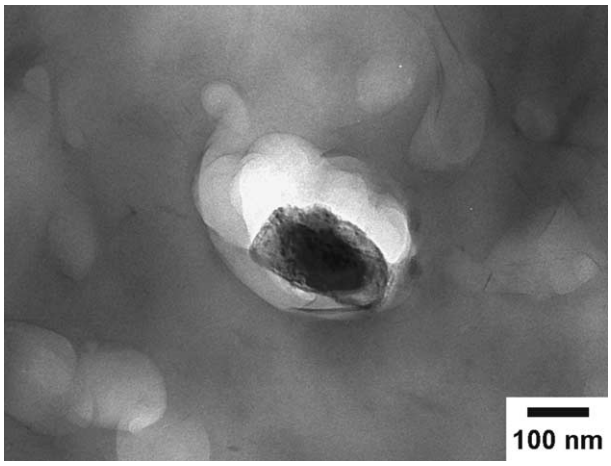

Fig. 1. TEM photomicrograph of a clay platelet pulled out by microtoming a polyamide-based nanocomposite formed from exfoliation of aluminosilicate platelets of montmorillonite-based organoclays in a polyamide-6 matrix; from Ref. [1].

matrix may have complicated irregular shapes, which, in general, may not be well approximated by a single aspect ratio. The particles in such nanocomposites are most often thought of as circular disks, but an ellipsoidally shaped disk may be a better approximation to the in-plane particle shape.

A more general idealized particle shape that has not received significant attention in the composite literature is an ellipsoid where all three major axes are different, i.e. $a_1 \neq a_2 \neq a_3$, as suggested in Fig. 2. In this paper, we develop a theoretical analysis of the mechanical properties of composites containing such three dimensional elliptical inclusions, where we take $a_1 > a_2 > a_3$. These particles are characterized by a primary aspect ratio, $\alpha = a_1/a_3$, and a secondary aspect ratio, $\beta = a_1/a_2$.

2. Background and strategy

Our proposed model containing three-dimensional ellipsoidal particles combines the Eshelby's equivalent tensor with a Mori–Tanaka type model having two aspect ratios (α and β). The influence of the primary and secondary aspect ratios on the effective elastic moduli of composites containing unidirectionally aligned isotropic inclusions will be examined. It is assumed that the polymer and the inclusions are well bonded to each other with both having linearly elastic, isotropic, and homogeneous properties. Thus, the compatibility between phases is excellent and the interfacial strength is much larger than the cohesive strength of polymer matrix. Furthermore, the inclusions are assumed to be uniformly distributed. If the inclusions are completely aligned, the composites can be theoretically regarded as macroscopically homogeneous and transversely isotropic. Therefore, independent elastic constants of the matrix and the particles are needed as input data. The goal is to express the effective elastic moduli of the composite in terms of the geometry of the inclusions, α and β, and the mechanical properties of the two phases at various concentrations.

Eshelby [3] combined the eigenstrain with the equivalent inclusions and solved the elastic stress field in and around an ellipsoidal particle with an infinite matrix. Variational principles for solid-elasticity theory have been suggested by Hashin and Rosen [4] and by Hill [5] to limit the upper and the lower bounds for the effective mechanical properties of fiber-reinforced composites by using self-consistent theory.

Many semi-empirical and numerical approaches have been proposed to predict mechanical properties with aligned inclusions. A typical example is the Halpin–Tsai equations [6] which express the mechanical behavior of composites

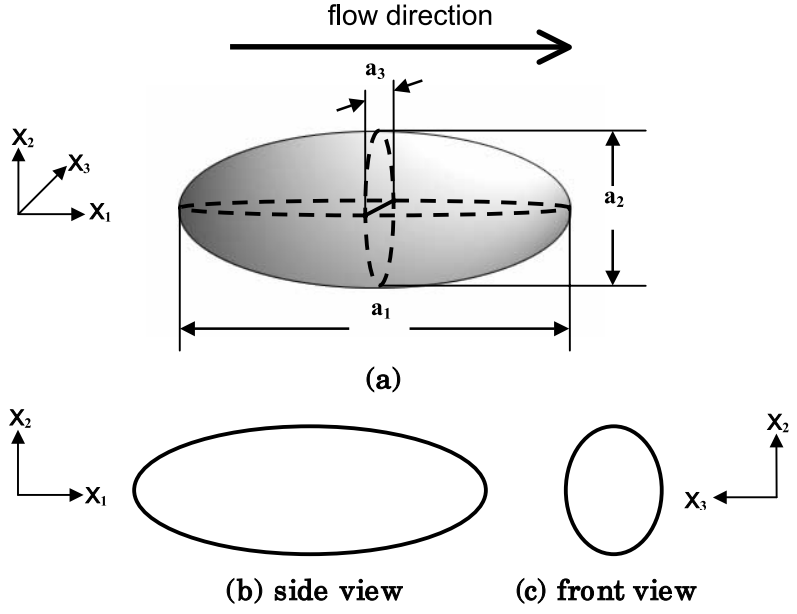

Fig. 2. Schematic views of a three dimensional ellipsoidal inclusion, where $a_1 > a_2 > a_3$, characterized by two aspect ratios: A primary aspect ratio $\alpha = a_1/a_3$ and a secondary aspect ratio $\beta = a_1/a_2$. Part (a) shows a three dimensional view, while part (b) shows a side view and part (c) shows a front view.

with unidirectional fiber orientation in terms of simple equations; a limited number of other shapes have been described by this approach. Chou et al. [7] applied Hill's method to analyze the elastic stiffness of short-fiber composites. By treating the inclusions and matrix separately, Russel [8] applied Eshelby's solution [3] to ellipsoidal inclusions; in spite of the fact that phase interactions were neglected, this result provides reasonable predictions at very dilute concentrations.

For systems with concentrations large enough to include an adequate number of inclusions within the elastic matrix but where there is enough distance between inclusions, the composite problem can be analyzed by combining Eshelby's solution [3] with Mori–Tanaka's average stress [9]. The main concept of this average stress is that under a given applied load, the average internal stress in the matrix is perturbed from the applied one due to the material containing filler particles with eigenstrains. The total integration of the localized stress of the perturbed parts over all the volume occupied by the composite comprised of the matrix and the particles has to vanish to zero in order to satisfy the equilibrium conditions. The Mori–Tanaka method and the nature of its approximation was reformulated and clarified by Benveniste [10]. The explicit expressions for the components of Eshelby's tensor were given by Mura [11] for various types of ellipsoidal inclusions. Tandon and Weng [12] applied these expressions to show the effects of inclusion shape or aspect ratio for the case of unidirectionally aligned flakes or short fibers. They described the theoretical approach for oblate and prolate spheroids using a two dimensional analysis of the five independent elastic constants for a transversely isotropic composite, i.e. for fiber-like, spherical, and disc-like inclusions. Calculations of composite properties were shown over the whole range of aspect ratio from zero to infinity. Recent papers have discussed the use of such composite theories to analyze the properties of clay-based nanocomposites [13,14].

In this paper, we follow the derivation developed by Tandon and Weng [12] and described by Tucker and Liang [15] in order to extend the basic theory to show how particles having two aspect ratios affect mechanical properties like the moduli and Poisson's ratio. The theoretical predictions will be shown as a function of the aspect ratios under conditions where the primary ratio is larger than the secondary one.

3. Basic theory

The basic theory needed to develop a model for composites containing inclusions characterized by two aspect ratios, specifically ellipsoidal particles without an axis of rotational symmetry, has been developed and published by many researchers; however, to our knowledge, there appear to be no published reports on such an extension of current theory. The works of Tandon and Weng [12] and the review paper by Tucker and Liang [15] were especially useful in the development of the model that follows.

Fig. 3(a) schematically illustrates the elements of the model to be used in the following analysis; it consists of oriented ellipsoidal inclusions embedded in an infinite, elastic matrix. For the ideal condition of uniform surface traction on the boundary of the composite, consistent stresses and strains can be defined as shown Fig. 3(b). There are contributions from both the matrix and the inclusions; the elastic modulus tensor for the matrix is denoted by $\mathbf{C}^{m}$, and that of the perfectly aligned ellipsoidal inclusions is given by $\mathbf{C}^{f}$. Generally, the constitutive equations for the inclusion and matrix material are

$$\boldsymbol{\sigma}^{f} = \mathbf{C}^{f}\boldsymbol{\varepsilon}^{f} \tag{1}$$

$$\boldsymbol{\sigma}^{m} = \mathbf{C}^{m}\boldsymbol{\varepsilon}^{m} \tag{2}$$

The local stress $\boldsymbol{\sigma}(\mathbf{x})$ and the local strain $\boldsymbol{\varepsilon}(\mathbf{x})$, which can be defined in Fig. 3(a) will, in general, not be uniform at the local position $\mathbf{x}$. The volume–average stress, $\bar{\boldsymbol{\sigma}}$, and strain, $\bar{\boldsymbol{\varepsilon}}$, can be determined by integrating the local quantities over a volume large enough to include an adequate number of inclusions

$$\bar{\boldsymbol{\sigma}} = \bar{\mathbf{C}}\bar{\boldsymbol{\varepsilon}} \tag{3}$$

where $\bar{\mathbf{C}}$ is the effective elastic modulus tensor of the composite. If the surface traction on the boundaries of the composite is assumed to be uniform or consistent with the uniform stress $\boldsymbol{\sigma}^{0}$ exerted on the surface of the volume, then the volume–average stress $\bar{\boldsymbol{\sigma}}$ can be regarded as a uniform stress $\boldsymbol{\sigma}^{0}$ in Fig. 3(b). In the composite, $\boldsymbol{\sigma}^{0}$ is the stress of the pure matrix $\boldsymbol{\sigma}^{m}$. Consequently, the uniform strain in the homogeneous matrix can be expressed as $\boldsymbol{\varepsilon}^{m}$ in the same way. So the strains of the composite and matrix material can be related as follows

$$\bar{\boldsymbol{\sigma}} = \boldsymbol{\sigma}^{m} \text{ and } \bar{\boldsymbol{\varepsilon}} = \boldsymbol{\varepsilon}^{m} \tag{4}$$

$$\bar{\boldsymbol{\sigma}} = \boldsymbol{\sigma}^{m} = \mathbf{C}^{m}\boldsymbol{\varepsilon}^{m} \tag{5}$$

The idea of stress- and strain-concentration tensors, $\mathbf{A}$ and $\mathbf{B}$, was introduced by Hill [17]. They are the requisite relationships between the average stress for the inclusions and the corresponding average stress for the composite. These relationships can be also applied to the average strain and stress

$$\boldsymbol{\varepsilon}^{f} = \mathbf{A}\bar{\boldsymbol{\varepsilon}} \tag{6}$$

$$\boldsymbol{\sigma}^{f} = \mathbf{B}\bar{\boldsymbol{\sigma}} \tag{7}$$

where $\mathbf{A}$ and $\mathbf{B}$ are the prerequisite fourth-order concentration tensors in the micromechanics of composite material problems.

In general, the average strain over an adequate system volume $\bar{\boldsymbol{\varepsilon}}$ is not exactly equal to $\boldsymbol{\varepsilon}^{m}$ due to the presence of

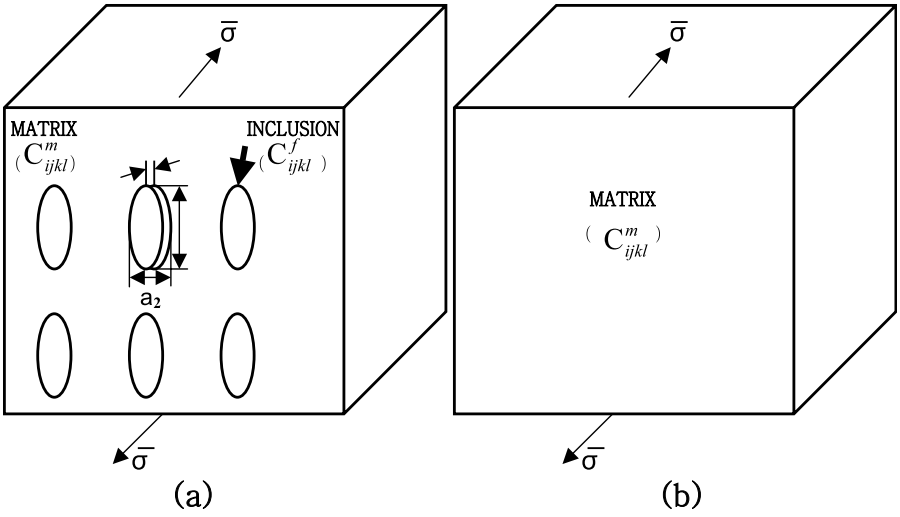

Fig. 3. A composite formed from aligned ellipsoidal inclusions ($a_1 > a_2 > a_3$) with two aspect ratios.

inclusions. This problem has to do with the perturbation strain $\tilde{\boldsymbol{\varepsilon}}^m$, which is the difference between the local strain and the average strain, and corresponds to an average perturbed stress denoted by $\tilde{\boldsymbol{\sigma}}^m$ in the matrix through the elastic constant $\mathbf{C}^m$, i.e.

$$\bar{\boldsymbol{\varepsilon}} = \boldsymbol{\varepsilon}^m + \tilde{\boldsymbol{\varepsilon}}^m \tag{8}$$

$$\tilde{\boldsymbol{\sigma}}^m = \mathbf{C}^m \tilde{\boldsymbol{\varepsilon}}^m \tag{9}$$

and

$$\bar{\boldsymbol{\sigma}} + \tilde{\boldsymbol{\sigma}}^m = \mathbf{C}^m(\boldsymbol{\varepsilon}^m + \tilde{\boldsymbol{\varepsilon}}^m) \tag{10}$$

The inclusions in the composite must have an additional perturbation strain, $\tilde{\boldsymbol{\varepsilon}}^f$, with the strain $\boldsymbol{\varepsilon}^m + \tilde{\boldsymbol{\varepsilon}}^m$ as follows

$$\bar{\boldsymbol{\varepsilon}} = \boldsymbol{\varepsilon}^m + \tilde{\boldsymbol{\varepsilon}}^m + \tilde{\boldsymbol{\varepsilon}}^f \tag{11}$$

The corresponding perturbed stress $\tilde{\boldsymbol{\sigma}}^f$ can be expressed as

$$\tilde{\boldsymbol{\sigma}}^f = \mathbf{C}^f \tilde{\boldsymbol{\varepsilon}}^f \tag{12}$$

Furthermore, the equivalent transformation strain of the inclusion, $\boldsymbol{\varepsilon}^t$, should be introduced according to Eshelby's equivalent principle. The stress equivalence between the inclusion and the composite may be expressed by

$$\begin{aligned}\bar{\boldsymbol{\sigma}} + \tilde{\boldsymbol{\sigma}}^m + \tilde{\boldsymbol{\sigma}}^f &= \mathbf{C}^f(\boldsymbol{\varepsilon}^m + \tilde{\boldsymbol{\varepsilon}}^m + \tilde{\boldsymbol{\varepsilon}}^f) \\ &= \mathbf{C}^m(\boldsymbol{\varepsilon}^m + \tilde{\boldsymbol{\varepsilon}}^m + \tilde{\boldsymbol{\varepsilon}}^f - \boldsymbol{\varepsilon}^t)\end{aligned} \tag{13}$$

The stiffness tensor of the matrix $\mathbf{C}^m$ was used instead of the stiffness tensor of the composite $\bar{\mathbf{C}}$. This concept was originally introduced by Mori and Tanaka [9]. Now, Eshelby's solution for the ellipsoidal inclusions can be applied to find the average stress and strain in the inclusions. Actually, the extra inclusion perturbation is related to the transformation strain through Eshelby's tensor which depends on the geometry of the inclusions; then the transformation strain tensor of Eq. (13) is assumed to be related to the Eshelby's tensor $\mathbf{S}$

$$\tilde{\boldsymbol{\varepsilon}}^f = \mathbf{S}\boldsymbol{\varepsilon}^t \tag{14}$$

The components of Eshelby's transformation tensor $\mathbf{S}$ are dependent upon the shape of the inclusions, Poisson's ratio, and the elastic modulus of the matrix; Mura gave expressions for inclusions of various geometries [11]. The appropriate components for inclusions with spherical, fiber-like and disc-like shapes were used by Tandon and Weng [12]. In this paper, we used the components for a three dimensional ellipsoidal shape with complex inclusions with no axes of symmetry where $a_1 > a_2 > a_3$.

By requiring the average perturbed stresses over the matrix and inclusions to go to zero with the applied average stress $\bar{\boldsymbol{\sigma}}$, we get

$$\tilde{\boldsymbol{\sigma}}^m + \phi\tilde{\boldsymbol{\sigma}}^f = 0 \tag{15}$$

where ϕ is the volume fraction of the inclusions. From Eqs. (8)–(10) and (13), we obtain the following simple expression

$$\tilde{\boldsymbol{\sigma}}^f = \mathbf{C}^m(\tilde{\boldsymbol{\varepsilon}}^f - \boldsymbol{\varepsilon}^t) \tag{16}$$

From Eqs. (9), (10), (15) and (16), we can rearrange the average perturbed strain in the matrix in terms of an arbitrary $\mathbf{C}^m$

$$\tilde{\boldsymbol{\varepsilon}}^m = -\phi(\tilde{\boldsymbol{\varepsilon}}^f - \boldsymbol{\varepsilon}^t) \tag{17}$$

For a given composite system, the average strain of the composite over its matrix and inclusions, $\bar{\boldsymbol{\varepsilon}}$ in Eq. (3), is related to the volume content of inclusions as follows

$$\bar{\boldsymbol{\varepsilon}} = \boldsymbol{\varepsilon}^m + \tilde{\boldsymbol{\varepsilon}}^m + \phi\tilde{\boldsymbol{\varepsilon}}^f \tag{18}$$

From Eqs. (17) and (18), we can finally get

$$\bar{\boldsymbol{\varepsilon}} = \boldsymbol{\varepsilon}^m + \phi\tilde{\boldsymbol{\varepsilon}}^t \tag{19}$$

The equivalent transformation strain $\tilde{\boldsymbol{\varepsilon}}^t$ will have to be found from the second part of Eq. (13). Next, the average strain $\bar{\boldsymbol{\varepsilon}}$

can be calculated by the consistent strain of the pure matrix $\boldsymbol{\varepsilon}^{\mathrm{m}}$ from Eq. (19).

4. Calculation of $\varepsilon_{ij}^{\mathrm{t}}$

The three dimensional ellipsoidal inclusions with no axes of symmetry are assumed to be aligned along the directions x_1, x_2 and x_3 as shown in Fig. 2. The components of Eshelby's transformation tensor, S_{ijkl} for this case, can be written as shown in Appendix A. They are dependent upon the aspect ratios α and β of the ellipsoidal inclusions and the Poisson's ratio of the matrix and can be expressed in terms of normal and shear components, exclusively. The elliptical integrals of the first and the second kinds, which are needed for Eshelby's tensor for particles of ellipsoidal shape, are shown in Appendix B.

The fourth-order stiffness tensors of both the matrix, C_{ijkl}^{m}, in Eq. (1) and the inclusions, C_{ijkl}^{f}, in Eq. (2) may be regarded as isotropic materials, respectively, and expressed by

$$C_{ijkl}^{\mathrm{m}} = \lambda_{\mathrm{m}}\delta_{ij}\delta_{kl} + \mu_{\mathrm{m}}(\delta_{ik}\delta_{jl} + \delta_{il}\delta_{jk}) \tag{20}$$

$$C_{ijkl}^{\mathrm{f}} = \lambda_{\mathrm{f}}\delta_{ij}\delta_{kl} + \mu_{\mathrm{f}}(\delta_{ik}\delta_{jl} + \delta_{il}\delta_{jk}) \tag{21}$$

where λ_{m}, μ_{m} and λ_{f}, μ_{f} are the Lame' constants of the matrix and inclusions, respectively, and δ_{ij} is the Kronecker delta. Eqs. (20) and (21) employ the Einstein summation convention for a repeated index from 1 to 3.

By use of Eqs. (13), (14) and (17), the equivalent transformation strain $\tilde{\boldsymbol{\varepsilon}}^{\mathrm{t}}$ can be expressed as

$$\left(C_{ijkl}^{\mathrm{f}} - C_{ijkl}^{\mathrm{m}}\right)\left[\varepsilon_{kl}^{\mathrm{m}} + (1-\phi)S_{klmn}\varepsilon_{mn}^{\mathrm{t}} + \phi\varepsilon_{kl}^{\mathrm{t}}\right] + C_{ijkl}^{\mathrm{m}}\varepsilon_{kl}^{\mathrm{t}} = 0 \tag{22}$$

Eq. (22) allows us to calculate $\varepsilon_{kl}^{\mathrm{t}}$ in terms of known parameters, such as $\varepsilon_{kl}^{\mathrm{m}}$, ϕ, C_{ijkl}^{m}, C_{ijkl}^{f} and S_{klmn}. To express the fourth-order stiffness tensors as a simplified index, we introduce the following notation, C_{IJ}^{m} from C_{ijkl}^{m}.

$$C_{ijkl}^{\mathrm{m}} \leftrightarrow C_{IJ}^{\mathrm{m}} \tag{23}$$

$$(ijkl) \leftrightarrow IJ$$

$$(ij) \leftrightarrow I$$

$$(11) \leftrightarrow 1, \quad (22) \leftrightarrow 2, \quad (33) \leftrightarrow 3$$

$$(12) = (21) \leftrightarrow 4, \quad (13) = (31) \leftrightarrow 5, \quad (23) = (32) \leftrightarrow 6$$

The simplified C_{IJ}^{m} enables us to visualize the tensor as a two-dimensional matrix; Eshelby's tensor and the shear strain tensor can be expressed in the same way

$$\left(C_{IJ}^{\mathrm{f}} - C_{IJ}^{\mathrm{m}}\right)\left[\varepsilon_{J}^{\mathrm{m}} + (1-\phi)S_{JK}\varepsilon_{K}^{\mathrm{t}} + \phi\varepsilon_{J}^{\mathrm{t}}\right] + C_{IJ}^{\mathrm{m}}\varepsilon_{J}^{\mathrm{t}} = 0 \tag{24}$$

Using Eshelby's tensor for inclusions with an ellipsoid-like shape from Appendix A with the stiffness tensors of both the matrix, C_{IJ}^{m}, and the inclusions, C_{IJ}^{f}, Eq. (24) is rearranged into the linear simultaneous equations, and are expressed by the matrix M_{IJ} as follows

$$M_{IJ}\varepsilon_{I}^{\mathrm{t}} = M_{I7}, \quad (I \text{ and } J = 1, 2, \ldots, 6) \tag{25}$$

$$\begin{bmatrix} M_{11} & M_{12} & M_{13} & 0 & 0 & 0 \\ M_{21} & M_{22} & M_{23} & 0 & 0 & 0 \\ M_{31} & M_{32} & M_{33} & 0 & 0 & 0 \\ 0 & 0 & 0 & M_{44} & 0 & 0 \\ 0 & 0 & 0 & 0 & M_{55} & 0 \\ 0 & 0 & 0 & 0 & 0 & M_{66} \end{bmatrix} \begin{bmatrix} \varepsilon_1^{\mathrm{t}} \\ \varepsilon_2^{\mathrm{t}} \\ \varepsilon_3^{\mathrm{t}} \\ \varepsilon_4^{\mathrm{t}} \\ \varepsilon_5^{\mathrm{t}} \\ \varepsilon_6^{\mathrm{t}} \end{bmatrix} = \begin{bmatrix} M_{17} \\ M_{27} \\ M_{37} \\ M_{47} \\ M_{57} \\ M_{67} \end{bmatrix} \tag{26}$$

where

$$M_{11} = \phi D_1 + D_2 + (1-\phi)(D_1 S_{11} + S_{21} + S_{31})$$

$$M_{12} = \phi + D_3 + (1-\phi)(D_1 S_{12} + S_{22} + S_{32})$$

$$M_{13} = \phi + D_3 + (1-\phi)(D_1 S_{13} + S_{23} + S_{33})$$

$$M_{21} = \phi + D_3 + (1-\phi)(S_{11} + D_1 S_{21} + S_{31})$$

$$M_{22} = \phi D_1 + D_2 + (1-\phi)(S_{12} + D_1 S_{22} + S_{32})$$

$$M_{23} = \phi + D_3 + (1-\phi)(S_{13} + D_1 S_{23} + S_{33})$$

$$M_{31} = \phi + D_3 + (1-\phi)(S_{11} + S_{21} + D_1 S_{31})$$

$$M_{32} = \phi + D_3 + (1-\phi)(S_{12} + S_{22} + D_1 S_{32})$$

$$M_{33} = \phi D_1 + D_2 + (1-\phi)(S_{13} + S_{23} + D_1 S_{33})$$

$$M_{44} = \phi + 2(1-\phi)S_{44} + \frac{\mu_{\mathrm{m}}}{\mu_{\mathrm{f}} - \mu_{\mathrm{m}}}$$

$$M_{55} = \phi + 2(1-\phi)S_{55} + \frac{\mu_{\mathrm{m}}}{\mu_{\mathrm{f}} - \mu_{\mathrm{m}}}$$

$$M_{66} = \phi + 2(1-\phi)S_{66} + \frac{\mu_{\mathrm{m}}}{\mu_{\mathrm{f}} - \mu_{\mathrm{m}}}$$

$$M_{17} = -\left(D_1\varepsilon_1^{\mathrm{m}} + \varepsilon_2^{\mathrm{m}} + \varepsilon_3^{\mathrm{m}}\right)$$

$$M_{27} = -\left(\varepsilon_1^{\mathrm{m}} + D_1\varepsilon_2^{\mathrm{m}} + \varepsilon_3^{\mathrm{m}}\right)$$

$$M_{37} = -\left(\varepsilon_1^{\mathrm{m}} + \varepsilon_2^{\mathrm{m}} + D_1\varepsilon_3^{\mathrm{m}}\right)$$

$$M_{47} = -\varepsilon_4^{\mathrm{m}}, \quad M_{57} = -\varepsilon_5^{\mathrm{m}}, \quad M_{67} = -\varepsilon_6^{\mathrm{m}}$$

and

$$D_1 = 1 + \frac{2(\mu_{\mathrm{f}} - \mu_{\mathrm{m}})}{(\lambda_{\mathrm{f}} - \lambda_{\mathrm{m}})}$$

$$D_2 = \frac{(\lambda_{\mathrm{m}} + 2\mu_{\mathrm{m}})}{(\lambda_{\mathrm{f}} - \lambda_{\mathrm{m}})}$$

$$D_3 = \frac{\lambda_{\mathrm{m}}}{\lambda_{\mathrm{f}} - \lambda_{\mathrm{m}}}$$

The components of the six by six square matrix M_{IJ} consist of known parameters that can be used to calculate the equivalent transformation strain $\varepsilon_I^{\mathrm{t}}$.

By using an appropriate numerical method, the terms of Eq. (26) can be solved simultaneously to obtain $\varepsilon_I^{\mathrm{t}}$, ($I=1$, 2,…,6). We can rewrite Eq. (19) to get the effective strain ($\bar{\boldsymbol{\varepsilon}} = \bar{\varepsilon}_I$)

$$\bar{\varepsilon}_I = \varepsilon_I^{\mathrm{m}} + \phi\varepsilon_I^{\mathrm{t}} \tag{27}$$

Finally, the effective elastic moduli of the composite can be calculated from Eqs. (3), (5), (25), and (27). Actually, the square matrix M_{IJ} in Eq. (26) can be numerically solved as a three by three matrix.

5. The elastic moduli

Composite materials have six components of moduli when the isotropic inclusions are aligned along the axis directions: The longitudinal Young's modulus E_{11}, the transverse Young's moduli E_{22} and E_{33}, and the shear moduli μ_{12}, μ_{13} and μ_{23}. These properties of composites can be determined from Eq. (26), Eq. (27) and the basic relationships under appropriate boundary conditions. Furthermore, Poisson's ratio, ν_{12}, can be obtained easily.

5.1. Longitudinal Young's, modulus E_{11}

In order to calculate E_{11}, the modulus tensor can be replaced by the compliance tensor, i.e. Eq. (28), to get

$$\bar{\varepsilon}_{ij} = C_{ijkl}^{-1}\bar{\sigma}_{kl} \tag{28}$$

or

$$\bar{\varepsilon}_I = C_{IJ}^{-1}\bar{\sigma}_J \tag{29}$$

To determine the longitudinal Young's modulus E_{11} with the compliance tensor matrix, C_{ijkl}^{-1} from Eq. (28), we apply a longitudinal normal stress $\bar{\sigma}_{11}$ with all other $\bar{\sigma}_{ij} = 0$. The average strain in the x_1 direction, $\bar{\varepsilon}_{11}$ of Eq. (28) becomes

$$\bar{\varepsilon}_{11} = E_{11}^{-1}\bar{\sigma}_{11} \tag{30}$$

The reference strains of Eq. (1) in the polymer matrix are

$$\varepsilon_{11}^{\mathrm{m}} = E_{\mathrm{m}}^{-1}\bar{\sigma}_{11} \text{ and } \varepsilon_{22}^{\mathrm{m}} = \varepsilon_{33}^{\mathrm{m}} = -\nu_{\mathrm{m}}E_{\mathrm{m}}^{-1}\bar{\sigma}_{11} \tag{31}$$

where ν_{m}, $\varepsilon_{11}^{\mathrm{m}}$ and E_{m} are the Poisson's ratio, the strain in the x_1 direction, and Young's modulus of the polymer matrix, respectively. Then, from Eqs. (30) and (31), the longitudinal effective modulus of the composite material E_{11} becomes

$$E_{11} = E_{\mathrm{m}}\varepsilon_{11}^{\mathrm{m}}(\bar{\varepsilon}_{11})^{-1} \tag{32}$$

Furthermore, from the above loading condition and the basic relation given by Eq. (28) for the compliance tensor, we easily get the equations for the Poisson's ratios for the composite, ν_{12} and ν_{13},

$$\bar{\varepsilon}_{22} = -\nu_{12}E_{11}^{-1}\bar{\sigma}_{11} \tag{33}$$

$$\bar{\varepsilon}_{33} = -\nu_{13}E_{11}^{-1}\bar{\sigma}_{11} \tag{34}$$

5.2. Transverse Young's modulus E_{22}

Similarly, to determine the transverse Young's modulus E_{22} in the x_2 direction for composites with the compliance tensor from Eq. (28), we apply a transverse normal stress $\bar{\sigma}_{22}$ in the x_2 direction with all other $\bar{\sigma}_{ij} = 0$; the resulting equation is

$$\bar{\varepsilon}_{22} = E_{22}^{-1}\bar{\sigma}_{22} \tag{35}$$

The strains in the x_2-direction of polymer matrix are

$$\varepsilon_{22}^{\mathrm{m}} = E_{\mathrm{m}}^{-1}\bar{\sigma}_{22} \text{ and } \varepsilon_{11}^{\mathrm{m}} = \varepsilon_{33}^{\mathrm{m}} = -\nu_{\mathrm{m}}E_{\mathrm{m}}^{-1}\bar{\sigma}_{22} \tag{36}$$

Then, in the x_2 direction, the transverse effective modulus of the composite material E_{22}, becomes

$$E_{22} = E_{\mathrm{m}}\varepsilon_{22}^{\mathrm{m}}(\bar{\varepsilon}_{22})^{-1} \tag{37}$$

5.3. Transverse Young's modulus E_{33}

Similarly, to determine the x_3 direction transverse Young's modulus E_{33} for the composite from Eq. (28) with the compliance tensor, we apply a transverse normal stress $\bar{\sigma}_{33}$ in the x_3 direction with all other $\bar{\sigma}_{ij} = 0$; the resulting equations are

$$\bar{\varepsilon}_{33} = E_{33}^{-1}\bar{\sigma}_{33} \tag{38}$$

The strains in the x_3 direction of polymer matrix are

$$\varepsilon_{33}^{\mathrm{m}} = E_{\mathrm{m}}^{-1}\bar{\sigma}_{33} \text{ and } \varepsilon_{11}^{\mathrm{m}} = \varepsilon_{22}^{\mathrm{m}} = -\nu_{\mathrm{m}}E_{\mathrm{m}}^{-1}\bar{\sigma}_{33} \tag{39}$$

In the x_3 direction, the transverse effective modulus of the composite material E_{33} becomes

$$E_{33} = E_{\mathrm{m}}\varepsilon_{33}^{\mathrm{m}}(\bar{\varepsilon}_{33})^{-1} \tag{40}$$

5.4. Shear moduli μ_{12}, μ_{13}, and μ_{23}

When we apply a pure shear stress $\bar{\sigma}_{12}$ and/or $\bar{\sigma}_{21}$, we can get the shear modulus μ_{12} by use of the effective strains obtained from Eqs. (26)–(28). From the compliance tensor of the composite of Eq. (28), we get the following relation

$$\bar{\varepsilon}_{12} = \bar{\varepsilon}_{21} = (2\mu_{12})^{-1}\bar{\sigma}_{12} = (2\mu_{21})^{-1}\bar{\sigma}_{21} \tag{41}$$

and for the pure matrix material

$$\varepsilon^{\mathrm{m}}_{12} = \varepsilon^{\mathrm{m}}_{21} = (2\mu_{\mathrm{m}})^{-1}\bar{\sigma}_{12} = (2\mu_{\mathrm{m}})^{-1}\bar{\sigma}_{21} \tag{42}$$

where μ_{m} is the shear modulus of pure matrix material. From Eqs. (20), (26), (27), (41) and (42), we get

$$\frac{\mu_{12}}{\mu_{\mathrm{m}}} = 1 + \frac{\phi}{2(1-\phi)S_{44} + \frac{\mu_{\mathrm{m}}}{\mu_{\mathrm{f}}-\mu_{\mathrm{m}}}} \tag{43}$$

In the same way, we obtain the shear moduli μ_{13}, and μ_{23} as follows

$$\frac{\mu_{13}}{\mu_{\mathrm{m}}} = 1 + \frac{\phi}{2(1-\phi)S_{55} + \frac{\mu_{\mathrm{m}}}{\mu_{\mathrm{f}}-\mu_{\mathrm{m}}}} \tag{44}$$

$$\frac{\mu_{23}}{\mu_{\mathrm{m}}} = 1 + \frac{\phi}{2(1-\phi)S_{66} + \frac{\mu_{\mathrm{m}}}{\mu_{\mathrm{f}}-\mu_{\mathrm{m}}}} \tag{45}$$

5.5. Poisson's ratio ν_{12}

To determine the Poisson's ratio ν_{12}, we need the same condition as the longitudinal normal stress $\bar{\sigma}_{11}$ with all other $\bar{\sigma}_{ij} = 0$. As Tucker and Liang suggested in Appendix A of their paper [15], the Poisson's ratio, ν_{12} can easily be of obtained from Eq. (33)

$$\nu_{12} = -\bar{\varepsilon}_{22}\cdot E_{11}\cdot(\bar{\sigma}_{11})^{-1} = -\frac{\bar{\varepsilon}_{22}}{\bar{\varepsilon}_{11}} \text{ or } \frac{\nu_{12}}{\nu_{\mathrm{m}}}$$
$$= \bar{\varepsilon}_{22}\cdot E_{11}\cdot(\varepsilon^{\mathrm{m}}_{22}\cdot E_{\mathrm{m}})^{-1} \tag{46}$$

and from Eq. (34), we get the Poisson's ratio, ν_{13}. By the same method, we can get the Poisson's ratios ν_{21}, ν_{23}, ν_{31} and ν_{32}.

6. Numerical method

Numerical calculations are executed using the flow chart shown in Fig. 4. First, the Eshelby's tensor is assigned with elliptical functions integrated from 0 to θ by Simpson's method. Next, the fourth order tensor is lowered to a second order tensor and becomes a six by six square matrix as illustrated by Eq. (26). Finally, the Gauss–Jordan method is used to solve the matrix M^{m}_{IJ}, which becomes an augmented matrix in the numerical method, to get the equivalent transformation strains $\varepsilon^{\mathrm{t}}_I$, $(I=1, 2,\ldots 6)$. The effective strains of composites $\bar{\varepsilon}_I$ are calculated from Eqs. (19) and (27). The calculated effective strains of the composite $\bar{\varepsilon}_I$ are expressed by $\bar{\varepsilon}_{ij}$ which are $\bar{\varepsilon}_{11}$, $\bar{\varepsilon}_{22}$, $\bar{\varepsilon}_{33}$, $\bar{\varepsilon}_{12}$, $\bar{\varepsilon}_{13}$, and $\bar{\varepsilon}_{23}$, according to Eq. (23). The material properties of composites can be calculated via the relationships of Section 5.

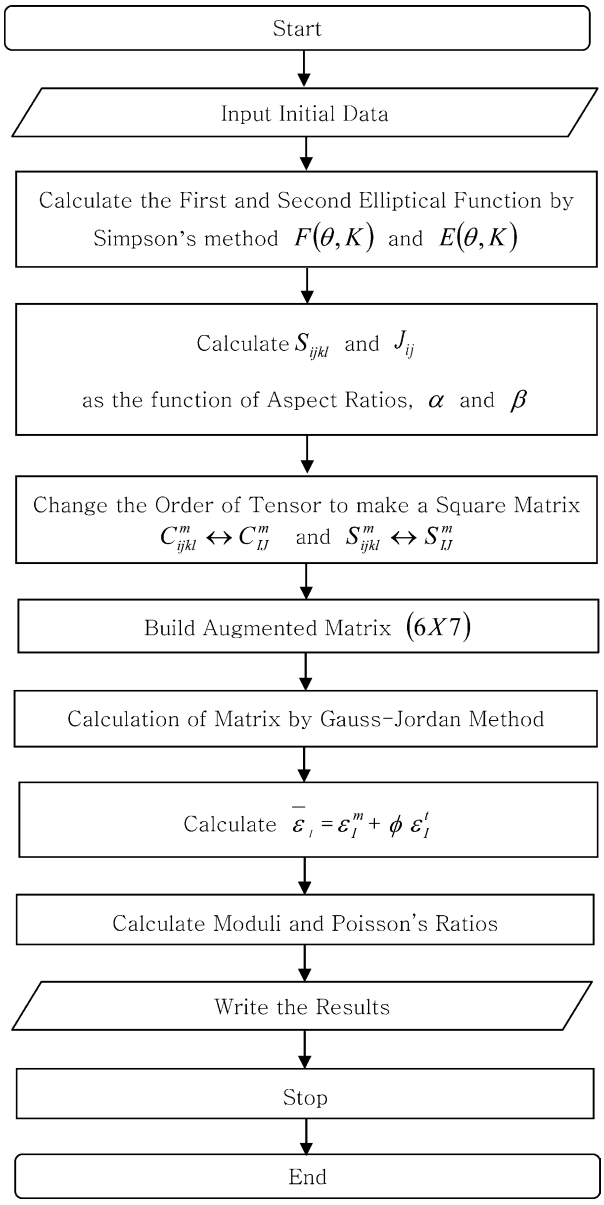

Fig. 4. Flow chart for numerical calculation of the elastic moduli from the model for a composite containing three dimensional ellipsoidal inclusions.

7. Numerical results and discussion

To show the effects of the aspect ratios, α and β and the volume fraction ϕ of inclusions on the six independent elastic moduli and Poisson's ratio, we use the characteristics of a fully-exfoliated montmorillonite/nylon 6 nanocomposite. The material properties of the nylon 6 matrix and the montmorillonite particles are assumed to be [13]

$E_{\mathrm{m}} = 2.75$ GPa, $\quad \nu_{\mathrm{m}} = 0.35$

$E_{\mathrm{f}} = 178$ GPa, $\quad \nu_{\mathrm{f}} = 0.20$

The homogeneous Young's moduli are denoted by E_{m} and E_{f}, while the Poisson's ratios are denoted as ν_{m} and ν_{f} where

the subscript (m) refers to the nylon 6 matrix and the subscript (f) refers to the montmorillonite filler.

First, the schematic views of sphere, disc, and fiber shaped inclusions are shown in Fig. 5, to define the axes of the shapes. The limiting cases of the three dimensional ellipsoidal model of Fig. 2 are a spherical shape where $\alpha = \beta = 1$ ($a_1 = a_2 = a_3$), a disc-like shape (abbreviation = MT-Disc, i.e. Mori–Tanaka disc) where $\beta = 1$ ($a_1 = a_2 \neq a_3$) and a fiber-like shape (abbreviation = MT-Fiber, i.e. Mori–Tanaka fiber) where $\alpha = \beta$ ($a_1 \neq a_2 = a_3$) given by the Mori–Tanaka model using the Tandon and Weng solution. The definition of the x_1-direction of E_{11} of the MT-Disc model in Fig. 5(b) is different from that of Gibbson [16]; here it is defined as the direction with the highest modulus.

The Young's moduli ratios of E_{11}/E_m (in the parallel direction) and E_{22}/E_m (in the perpendicular direction) are shown as a function of the secondary aspect ratio β ($= a_1/a_2$) for a primary aspect ratio $\alpha = 100$ and volume fraction $\phi = 0.04$ in Fig. 6. In the parallel direction, the modulus ratio E_{11}/E_m goes smoothly from a value of 2.36 of the disc-like shape of the MT-Disc model ($\beta = 1$) to a value of 3.40 given by the fiber-like shape of the MT-Fiber model ($\alpha = \beta$) in the Tandon and Weng solution, as β goes from 1 to 100. In the perpendicular direction, the modulus ratio of E_{22}/E_m goes smoothly from 2.36 for the disc-like shape to 1.16 for the fiber-like shape as β goes from 1 to 100.

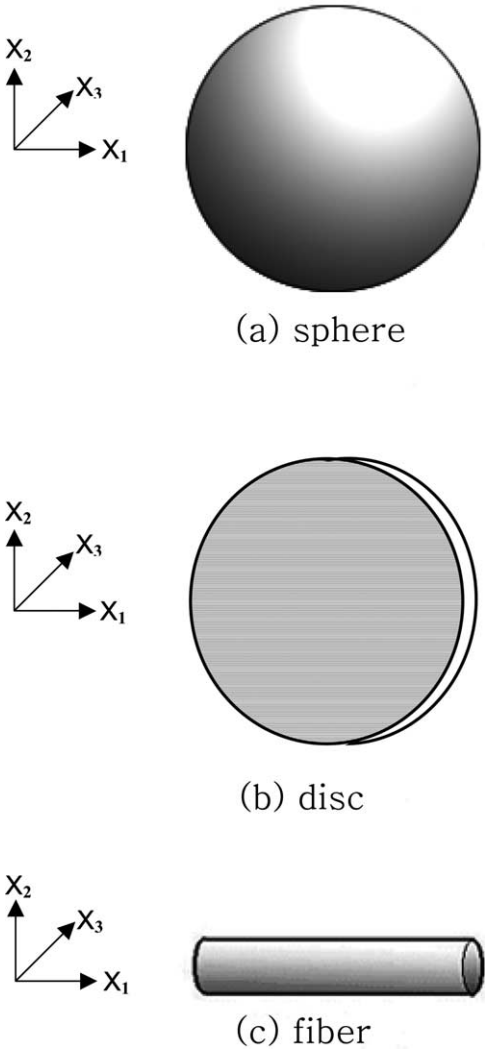

Fig. 5. Schematic views of inclusions with the shape of a sphere, disc, and fiber and their orientation relative to sample axes.

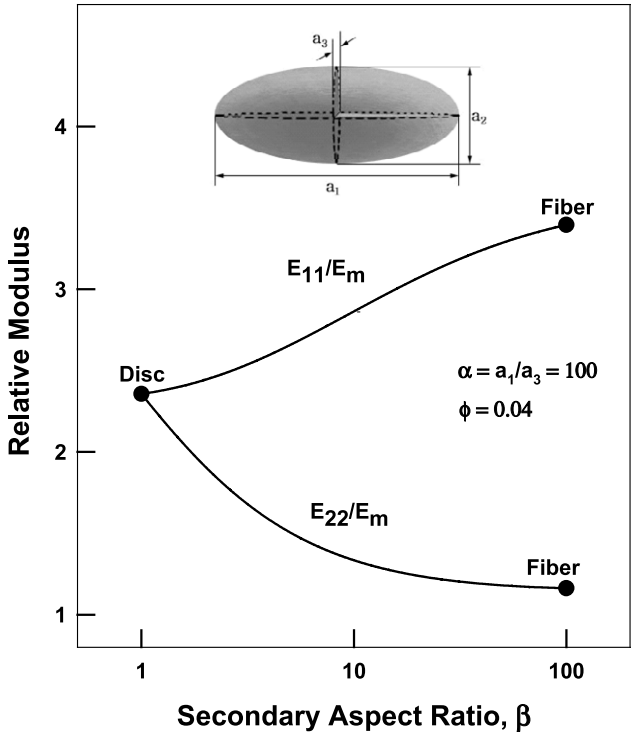

Fig. 6. Normalized Young's modulus, E_{11}/E_m in the parallel x_1 and perpendicular x_2 directions of a composite material as a function of the secondary aspect ratio, $\beta = a_1/a_2$, from unity (disc shaped inclusion) to $\beta = \alpha$ (fiber shaped inclusion) for a primary aspect ratio $\alpha = 100$ and $\phi = 0.04$.

It should be noted that the mathematical form of the current model leads to numerical difficulties in calculations in the exact limit of $a_1 = a_2$ or $\beta = 1$ since, the integrands of the forms for ω_1 in Appendix A go to infinity at the upper limit of the integration; of course, the integral itself is finite. This numerical difficulty can be avoided by use of a series expansion in this limit. When this numerical difficulty is eliminated in the manner suggested, the current model properly extrapolates to the value given by the MT-Disc model via the Tandon and Weng solution. Likewise, there is a similar problem at $a_2 = a_3$ or $\alpha = \beta$ with the integrand of the equation for ω_2 in Appendix A; however, again the results do approach the values given by MT-Fiber model in this limit, when this calculational difficulty is eliminated.

The calculated longitudinal Young's modulus E_{11} for a hypothetical nanocomposite composed of nylon 6 and filler is shown in Fig. 7 as a function of volume fraction of filler where the secondary aspect ratio varies from 1 to 150 when the primary aspect ratio is fixed at $\alpha = 150$. These plots are quite linear over a wide range of volume fraction; generally

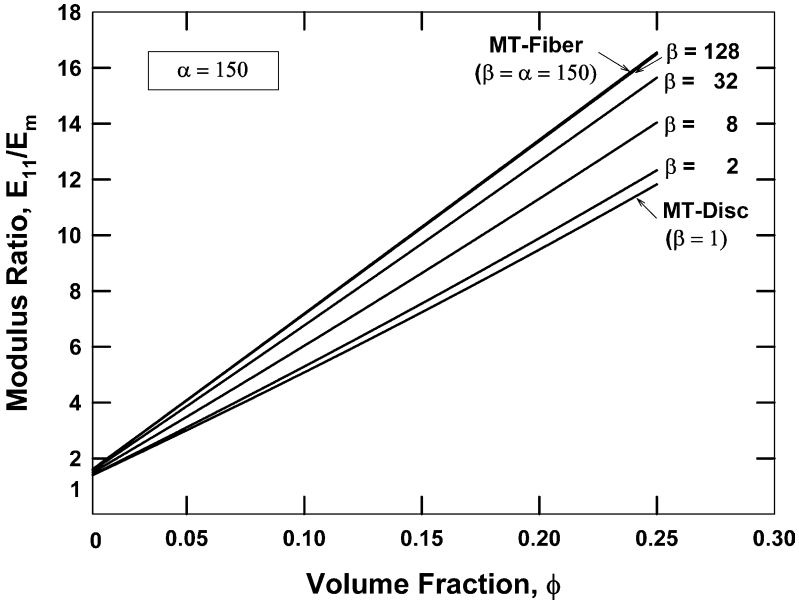

Fig. 7. Normalized Young's modulus, E_{11}/E_m, calculated from current model as a function of volume fraction where the secondary aspect ratio β varies from unity (disc shaped inclusion) to 150 (fiber shaped inclusion). The two extremes correspond to the Mori–Tanaka, MT, model for discs and fibers.

speaking, the volume fraction of montmorillonite in such nanocomposites would rarely be above 0.05. The modulus ratio E_{11}/E_m increases as the secondary aspect ratio increases; however, the rate of increase becomes less as the secondary aspect ratio increases. Note that for $\beta=128$ the modulus ratio is essentially the same as the value for the MT-Fiber where $\alpha=\beta=150$.

The longitudinal Young's modulus ratio E_{11}/E_m is shown in Fig. 8 as a function of the primary aspect ratio α ($=a_1/a_3$) for a given volume fraction $\phi=0.04$ and different values of the secondary aspect ratio $\beta(=a_1/a_2)$. The current model is also compared with the MT-Disc, MT-Fiber, and Halpin–Tsai (abbreviation=HT) models in Fig. 8. Increasing the secondary aspect ratio increases E_{11}/E_m, for a given α, from the lower limit of the MT-Disc model ($\beta=1$); but at $\beta=6$, the highest value shown, the modulus ratio is still below the prediction given by the Halpin–Tsai and, of course, the MT-Fiber limit ($\alpha=\beta$).

Fig. 9 shows the calculated Young's moduli in the three coordinate directions, i.e. E_{11}, E_{22}, and E_{33}, relative to that of the matrix for the composite as a function of the primary aspect ratio where the secondary aspect ratio is set to $\beta=3$ for a volume fraction $\phi=0.04$. The results are compared with the HT model, MT-Fiber, and MT-Disc models. For all

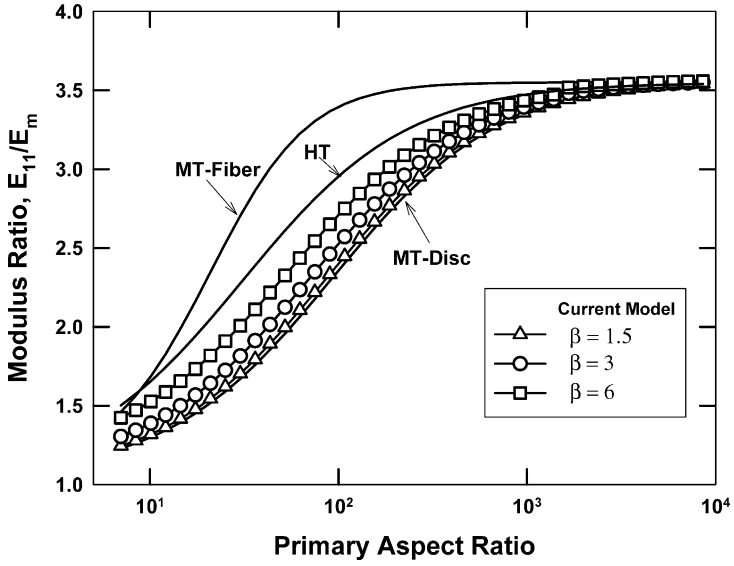

Fig. 8. Effect of the secondary aspect ratios on the longitudinal Young's modulus, E_{11}/E_m, calculated from the current model and comparisons with the Halpin–Tsai model (HT) and the Mori–Tanaka models for fibers (MT-Fiber) and discs (MT-Disc) at a volume fraction $\phi=0.04$ where $E_f=178$ GPa and $E_m=2.75$ GPa.

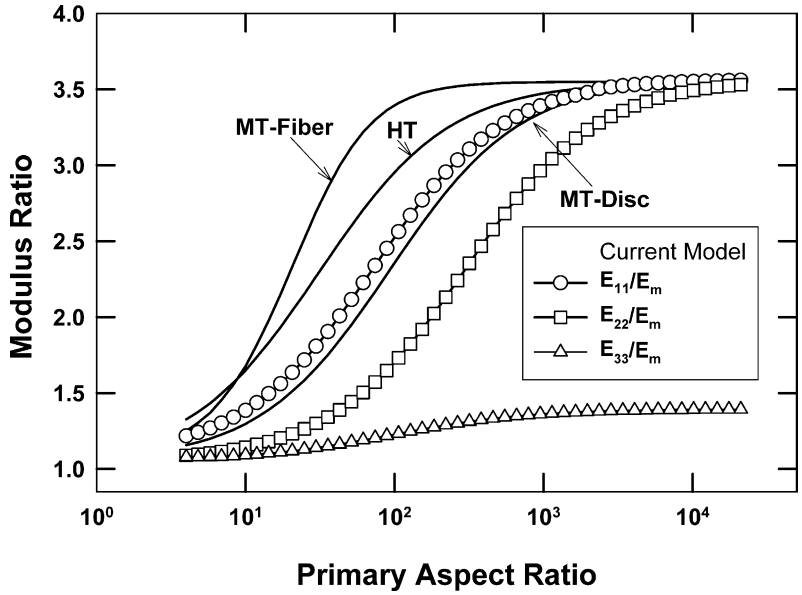

Fig. 9. Comparison of 3-dimensional ellipsoidal model with Halpin–Tsai model (HT) and Mori–Tanaka models for fibers (MT-Fiber) and discs (MT-Disc) as a function of the primary aspect ratio, α, for a fixed secondary aspect ratio $\beta=3$, volume fraction, $\phi=0.04$, $E_f=178$ GPa and $E_m=2.75$ GPa.

primary aspect ratios, the predicted longitudinal Young's modulus, E_{11}, from the current model is greater than that predicted by the MT-Disc model but less than that predicted by the MT-Fiber model as shown in Fig. 8.

The transverse Young's modulus E_{22} predicted by the current model, with $\beta=3$, is less than E_{11} from the MT-Disc model. The rate of increase for both curves is similar, as if one curve could be shifted to coincide with the other; of course, the deviations between the two curves are dependent upon the secondary aspect ratio ($\beta=3$). The most relevant aspect ratio for the transverse Young's modulus, or E_{22}, is α/β or a_2/a_3, in Fig. 9, $\alpha/\beta=\alpha/3$. The transverse modulus ratio predicted by the current model is approximately the same as the longitudinal modulus, or E_{11}, ratio predicted by the Mori–Tanaka Disc model with an aspect ratio of $\alpha/3$ (i.e. α/β); e.g. the transverse modulus ratio E_{22}/E_m is 1.732 at $\alpha=106.5$ from the current model (with $\beta=3$), while E_{11}/E_m is 1.752 at $\alpha=35.5$ from the MT-Disc model, see Fig. 9. Clearly, the transverse Young's modulus E_{22} predicted by the current model strongly depends on α/β or a_2/a_3. The Young's modulus in the third coordinate direction, E_{33}, as predicted by the current model increases similarly to E_{11} or E_{22}; however, the magnitude of the increase is much less as shown in Fig. 9.

The calculated longitudinal Young's modulus of the composite E_{11}, relative to that of the matrix, is shown in Fig. 10 as a function of the volume fraction for the case where the primary aspect ratio α is 10, 25, 100 and 500 with β fixed at 3 and where the secondary aspect ratio β is 1.5, 3 and 6 with the primary aspect ratio α fixed at 25. In this figure, the curves are drawn over the entire volume fraction range from 0 to 1 to show the non-linear nature of the relations at higher loadings or the inefficiency of the filler for providing reinforcement at low loading; of course, loadings beyond some point become experimentally difficult to form and eventually impossible because of theoretical packing limits for a dispersed phase. In all cases, the modulus, at a given filler content, increases as the primary and secondary aspect ratios, α and β increase.

The effect of the secondary aspect ratio, β, on the calculated longitudinal Young's modulus of the composite, E_{11}, is shown more clearly in Fig. 11 by plotting the modulus ratio versus the secondary aspect ratio β from $\beta=1$ to $\beta=\alpha$ for fixed values of the primary aspect ratio, α, from $\alpha=25$ to $\alpha=1600$ at a volume fraction $\phi=0.04$. The limits for a sphere (the point where $\alpha=\beta=1$), disc (the bold line along which $\beta=1$), and fiber (the bold line along which $\alpha=\beta$) shaped inclusions are shown in this presentation. The modulus always increases as the secondary aspect ratio, β, increases at a fixed primary aspect ratio. To illustrate this, for $\alpha=50$, the modulus ratio increases from 1.934 to 3.102 as β goes from $\beta=1$ to $\beta=50$. On the other hand, for $\beta=1$ and $\alpha=400$ (MT-Disc model) the modulus ratio is 3.092, while for $\beta=\alpha$ and $\alpha=50$ (MT-Fiber model) this ratio is nearly identical at 3.102. In more extreme cases, the modulus at a low primary aspect ratio, α, may be larger than that at a higher α due to the change of the secondary aspect ratio, β. Clearly, the secondary aspect ratio can have a considerable effect on the modulus E_{11} as shown in Figs. 10 and 11 and these examples.

The calculated transverse Young's modulus of the composite E_{22}, relative to that of the matrix is shown in Fig. 12 over the entire range of volume fractions for the following cases: $\alpha=10$, 25, 100 and 500 with β fixed at 3 and $\beta=1.5$, 3 and 6 with α fixed at 25. The transverse Young's modulus E_{22} increases as the primary aspect ratio increases in a similar manner shown above for E_{11}. However, E_{22} decreases as the secondary aspect ratio increases. An

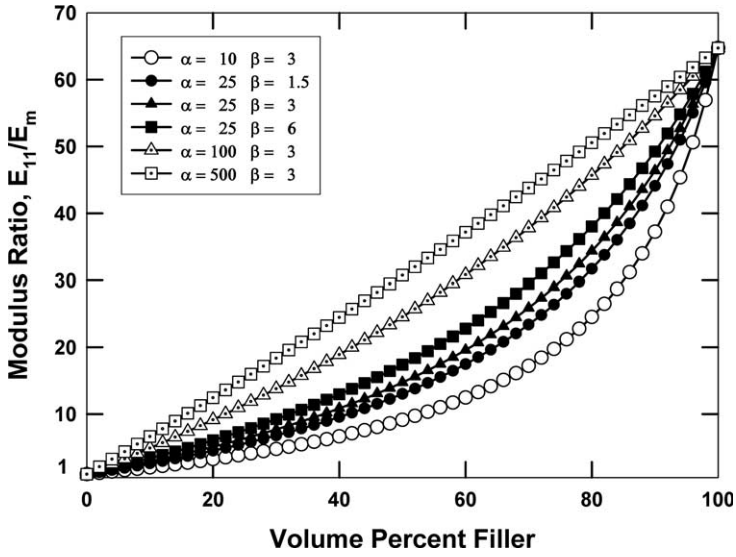

Fig. 10. Normalized longitudinal Young's modulus, E_{11}/E_m, predicted by the current model as a function of primary aspect ratio α and secondary aspect ratio β where $E_f = 178$ GPa and $E_m = 2.75$ GPa.

increase in the secondary aspect ratio, $\beta = a_1/a_2$, for a fixed primary aspect ratio, $\alpha = a_1/a_3$, means the length a_2 of inclusion in the x_2 direction must decrease for a fixed length a_3. Thus, the decreasing behavior of E_{22} with increasing β is physically understandable.

The relative transverse Young's modulus E_{22} of composites is shown in Fig. 13 as a function of secondary aspect ratio for fixed values of the primary aspect ratio and volume fraction $\phi = 0.04$ in analogous fashion as shown in Fig. 11 for E_{11}. Again, the limits for sphere, disc, and fiber shaped inclusions are shown. The transverse modulus decreases as the secondary aspect ratio β increases for a fixed primary aspect ratio α, e.g. at a primary aspect ratio $\alpha = 50$, the modulus ratio decreases from 1.934 to 1.158 as the secondary aspect ratio increases from $\beta = 1$ to $\beta = \alpha = 50$. The trend for E_{11} is the reverse of this.

From Fig. 12, we can get a sense of how the transverse modulus depends on the aspect ratio $a_2/a_3 = \alpha/\beta$. At $\phi = 0.10$, for $\alpha = 25$ and $\beta = 1.5$ or $\alpha/\beta = 16.67$, the modulus ratio is 2.108 and at $\alpha = 100$ and $\beta = 6$ or $\alpha/\beta = 16.67$, the modulus ratio is 2.109. The modulus ratios for these two cases, where $a_2/a_3 = \alpha/\beta$ are the same, are virtually identical. In some cases, it is useful to use the alternate aspect ratio, $a_2/a_3 = \alpha/\beta$, as shown for the plot of transverse

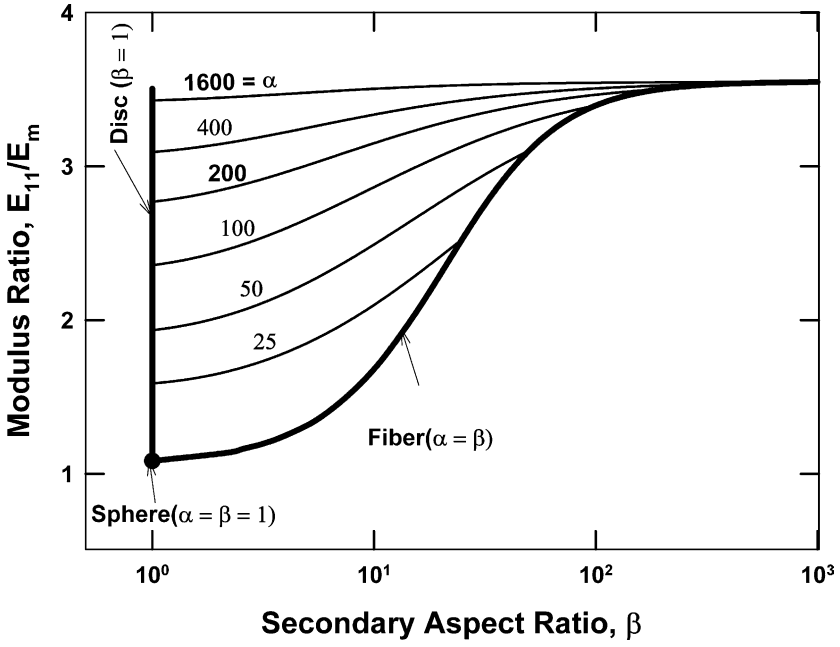

Fig. 11. Normalized longitudinal Young's modulus, E_{11}/E_m, as a function of the secondary aspect ratio, β, from unity (disc shaped inclusion) to $\beta = \alpha$ (fiber shaped inclusion) for various fixed primary aspect ratios.

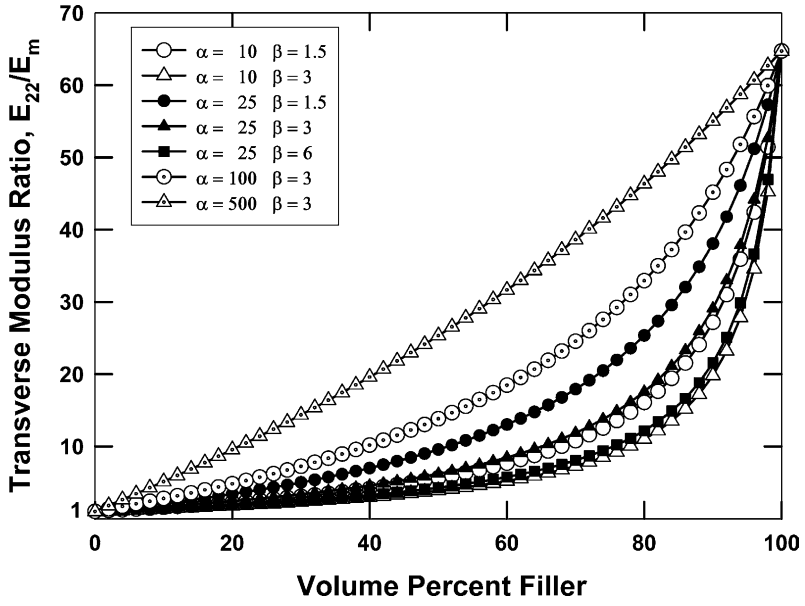

Fig. 12. Normalized transverse Young's modulus, E_{22}/E_m, predicted by the current model as a function of the primary aspect ratio α and the secondary aspect ratio β where $E_f = 178$ GPa and $E_m = 2.75$ GPa.

Young's modulus ratio E_{22}/E_m in Fig. 14. Here the reinforcement effect is shown as a function of the aspect ratio α/β for cases where the primary aspect ratios are 50, 500 and 5000 for a volume fraction $\phi = 0.04$; the three curves essentially collapse into one curve in Fig. 14 when plotted in this way. In other words, the modulus ratio E_{22}/E_m can be approximately expressed in terms of the single aspect ratio, α/β, in this region as shown in Fig. 14; whereas, in Fig. 13 two aspect ratios have to be specified to define the material properties in the x_2 direction.

The transverse Young's modulus of the composite E_{33}, relative to that of the matrix, calculated from the current model is shown in Fig. 15 as a function of the volume fraction of inclusions. The effects of the aspect ratios α and β on the transverse Young's modulus E_{33} are almost negligible and consistent with what is seen in Fig. 9.

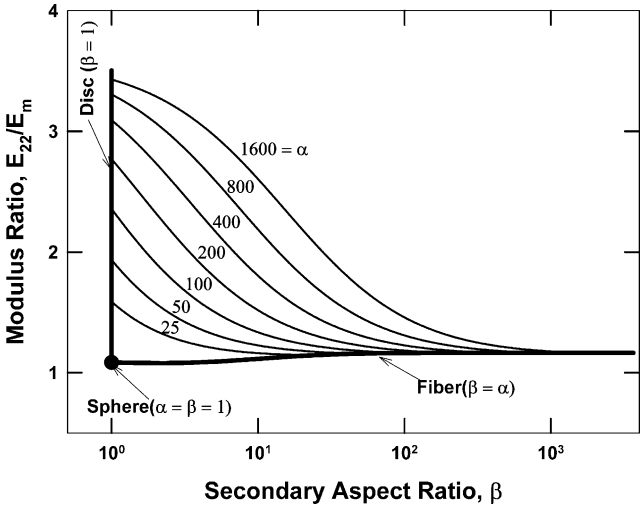

Fig. 13. Normalized transverse Young's modulus, E_{22}/E_m, as a function of the secondary aspect ratio from unity (disc shaped inclusion) to $\beta = \alpha$ (fiber shaped inclusion) for various fixed primary aspect ratios.

The calculated shear modulus of the composite μ_{12}, relative to the matrix shear modulus is shown in Fig. 16 as a function of the filler volume fraction for the cases $\alpha = 10$, 25, 100 and 500 with β fixed at 3 and $\beta = 1.5$, 3 and 6 with α fixed at 25. Note that μ_{12} describes the response of the composite to a shear stress in the x_2 direction acting in a plane of the normal vector of the x_1 direction and is identical to μ_{21}. The effects of aspect ratios on the shear modulus μ_{12} are similar to the effects on E_{22}. The shear modulus μ_{12} increases as the primary aspect ratio α increases, while it decreases as the secondary aspect ratio β increases. In Fig. 16, the shear moduli μ_{12} given by the curve defined by the open-circles where $\alpha = 10$ and $\beta = 1.5$ are larger than those given by the curve defined by the closed-squares where $\alpha = 25$ and $\beta = 6$ in Fig. 16. Analogous trends are seen in Fig. 12.

The shear modulus of composites μ_{12} relative to that of the matrix is shown in Fig. 17 as a function of secondary aspect ratio for fixed values of the primary aspect ratio and a volume fraction $\phi = 0.04$. The limiting cases for sphere, disc, and fiber shaped inclusions are shown in analogous fashion as in Figs. 11 and 13. The shear modulus decreases as the secondary aspect ratio β increases for a fixed primary aspect ratio α as also seen for the transverse Young's modulus E_{22}.

As shown earlier for E_{22}, the shear modulus of composites μ_{12} can be expressed approximately as a unique function of the alternate aspect ratio α/β as shown in Fig. 14. As before, the curves for the primary aspect ratios of 50, 500 and 5000 at a volume fraction $\phi = 0.04$ approximately collapse into a single function of α/β.

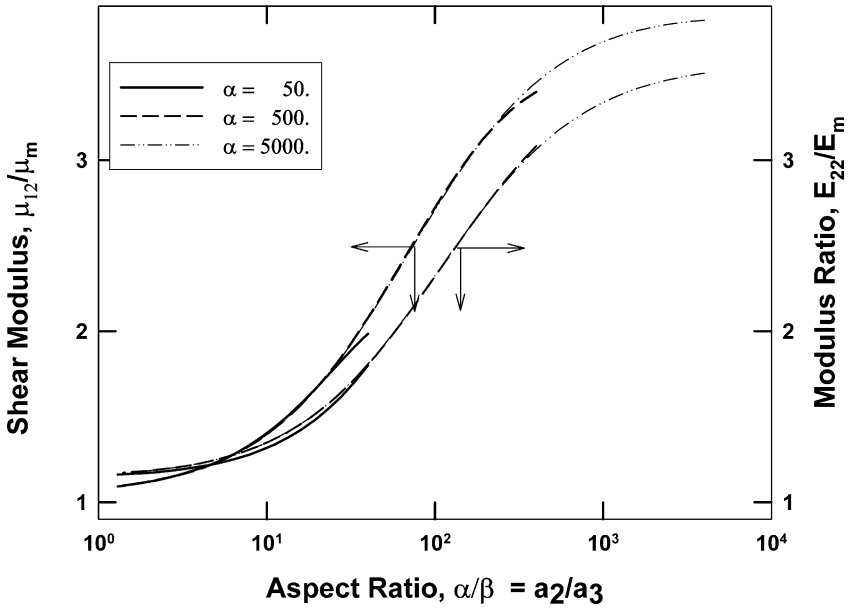

Fig. 14. Transverse Young's modulus E_{22} and shear modulus, μ_{12}, versus $\alpha/\beta = a_2/a_3$ with the constant primary aspect ratios of $\alpha = 50$, 500 and 5000.

The calculated shear moduli of the composite μ_{13} and μ_{23}, relative to that of the matrix, are shown in Figs. 18 and 19, respectively, as a function of the volume fraction for various combinations of α and β. Both shear moduli show similar trends; they decrease with increasing primary aspect ratio α but increase with increasing secondary aspect ratio β. The effects of aspect ratios on these shear moduli are relatively small compared with the effects on μ_{12}.

The Poisson's ratio calculated for the composite ν_{12}, as defined by Eq. (46) is shown in Fig. 20 as a function of the primary aspect ratio, with β fixed at 3, for various fixed volume fractions. Note that ν_{12} is defined as the negative ratio of the strain in the x_2 direction to the strain in the direction of the applied load, i.e. x_1 direction. This Poisson's ratio decreases as aspect ratio increases and as the volume fraction of the filler increases and approaches that of filler, $\nu_f = 0.20$, at high loadings and aspect ratios. These results are similar to those of Tandon and Weng [12].

8. Conclusion

A model for the mechanical properties of a composite consisting of perfectly aligned ellipsoidal particles having

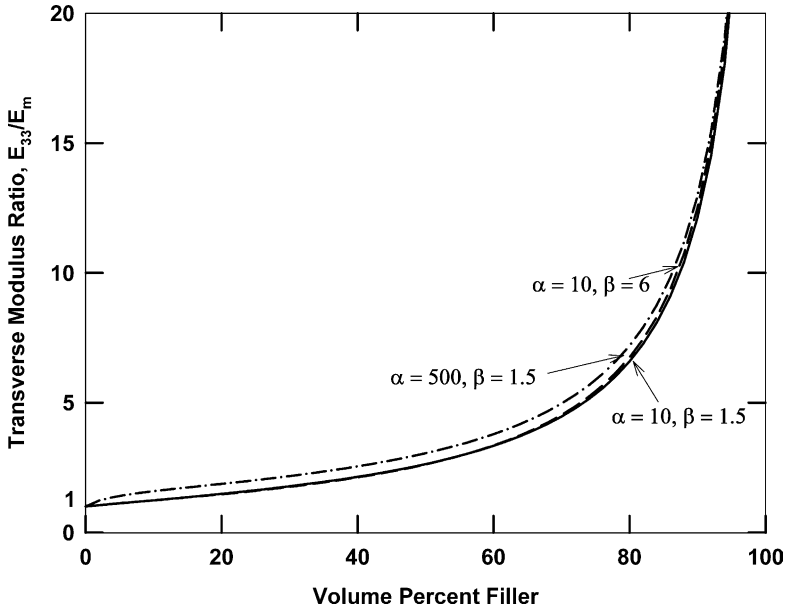

Fig. 15. Normalized transverse Young's modulus, E_{33}/E_m, predicted by the current model as a function of the primary aspect ratio α and the secondary aspect ratio β where $E_f = 178$ GPa and $E_m = 2.75$ GPa.

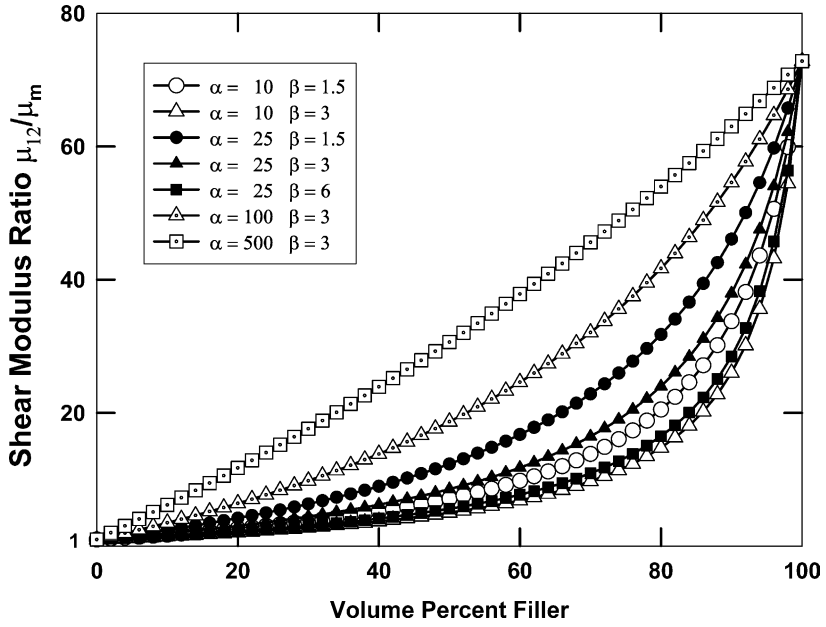

Fig. 16. Normalized shear modulus, μ_{12}/μ_m, calculated from the current model as a function of concentration where $\mu_f = 74.2$ GPa and $\mu_m = 1.02$ GPa.

no axis of rotational symmetry has been developed. The effects of the primary and secondary aspect ratios, α and β, on various moduli calculated by the current model, are compared with the predictions by the theoretical approaches of Halpin–Tsai and Mori–Tanaka. The current model permits predictions that correctly approach the limiting cases for a sphere (where $\alpha = \beta = 1$), disc (where $\beta = 1$), and fiber (where $\alpha = \beta$) shaped inclusions. The longitudinal Young's modulus E_{11} increases as both the primary and secondary aspect ratios increase. The E_{11} predicted by the current model increases from that of the MT-Disc model to that of the MT-Fiber model, as the secondary aspect ratio increases.

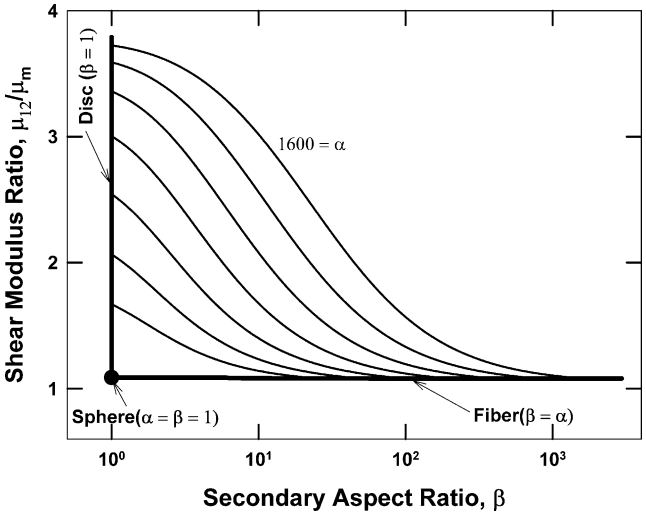

Fig. 17. Normalized shear modulus, μ_{12}/μ_m, as a function of the secondary aspect ratio from unity (disc shaped inclusion) to $\beta = \alpha$ (fiber shaped inclusion) for various fixed primary aspect ratios.

However, the transverse Young's modulus E_{22} decreases, as the secondary aspect ratio increases. The results can be approximately expressed as a function of the alternate aspect ratio α/β or a_2/a_3. The shear modulus of composites μ_{12} shows a similar trend as the transverse Young's modulus E_{22}.

Appendix A. Components of Eshelby's tensor S_{ijkl}

The components of Eshelby's tensor for a three dimensional ellipsoidal model that appropriately deals with complex inclusions with no axes of symmetry and are possibly irregular in shape can be derived from the explicit expressions of Mura [11]. For the ellipsoidal inclusion of the current model ($a_1 > a_2 > a_3$), where there are two different aspect ratios α and β, the components of Eshelby's tensor S_{ijkl} are given by

$$S_{1111} = \frac{3J_{11}}{8\pi(1-\nu_m)} + \frac{(1-2\nu_m)\omega_1}{8\pi(1-\nu_m)}$$

$$S_{1122} = \frac{J_{21}}{8\pi(1-\nu_m)} - \frac{(1-2\nu_m)\omega_1}{8\pi(1-\nu_m)}$$

$$S_{1133} = \frac{J_{31}}{8\pi(1-\nu_m)} - \frac{(1-2\nu_m)\omega_1}{8\pi(1-\nu_m)}$$

$$S_{2211} = \frac{J_{12}}{8\pi(1-\nu_m)} - \frac{(1-2\nu_m)(\omega_2-\omega_1)}{8\pi(1-\nu_m)}$$

$$S_{2222} = \frac{3J_{22}}{8\pi(1-\nu_m)} + \frac{(1-2\nu_m)(\omega_2-\omega_1)}{8\pi(1-\nu_m)}$$

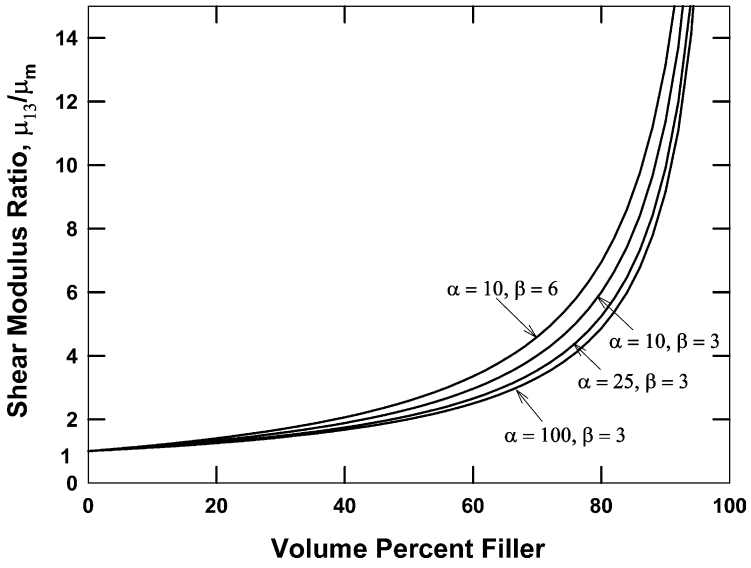

Fig. 18. Normalized shear modulus ratio, μ_{13}/μ_m, predicted by the current model as a function of concentration where $\mu_f = 74.2$ GPa and $\mu_m = 1.02$ GPa.

$$S_{2233} = \frac{J_{32}}{8\pi(1-\nu_m)} - \frac{(1-2\nu_m)(\omega_2-\omega_1)}{8\pi(1-\nu_m)}$$

$$S_{3311} = \frac{J_{13}}{8\pi(1-\nu_0)} - \frac{(1-2\nu_m)(4\pi-\omega_2)}{8\pi(1-\nu_m)}$$

$$S_{3322} = \frac{J_{23}}{8\pi(1-\nu_m)} - \frac{(1-2\nu_m)(4\pi-\omega_2)}{8\pi(1-\nu_m)}$$

$$S_{3333} = \frac{3J_{33}}{8\pi(1-\nu_m)} + \frac{(1-2\nu_m)(4\pi-\omega_2)}{8\pi(1-\nu_m)}$$

$$S_{1212} = S_{2112} = S_{1221} = S_{2121} = \frac{(J_{12}+J_{21})}{16\pi(1-\nu_m)} - \frac{(1-2\nu_m)}{16\pi(1-\nu_m)}(\omega_2)$$

$$S_{1313} = S_{3113} = S_{1331} = S_{3131} = \frac{(J_{13}+J_{31})}{16\pi(1-\nu_m)} - \frac{(1-2\nu_m)}{16\pi(1-\nu_m)}(4\pi+\omega_1-\omega_2)$$

$$S_{2323} = S_{3223} = S_{2332} = S_{3232} = \frac{(J_{23}+J_{32})}{16\pi(1-\nu_m)} - \frac{(1-2\nu_m)}{16\pi(1-\nu_m)}(4\pi-\omega_1)$$

$$S_{1112} = S_{1223} = S_{1232} = 0$$

In the above, ν_m is Poisson's ratio of the polymer matrix, and the terms J_{ij} are given by

$$J_{12} = \frac{\beta^2(\omega_2-2\omega_1)}{(\beta^2-1)}$$

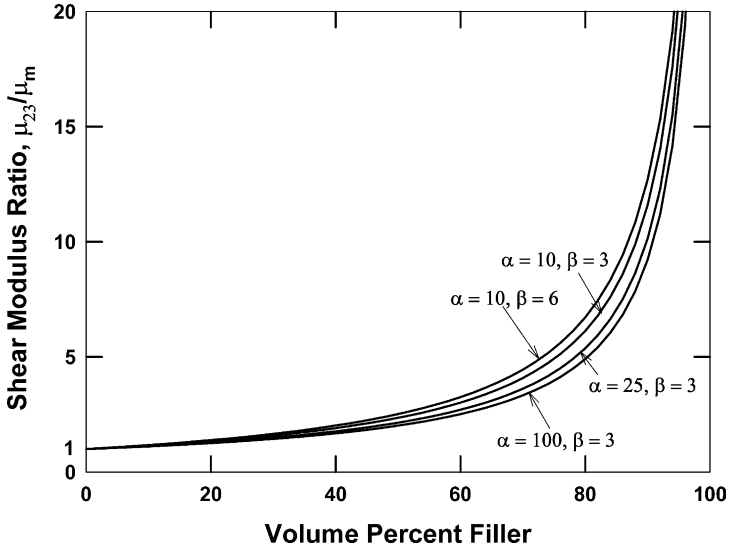

Fig. 19. Normalized shear modulus ratio, μ_{23}/μ_m, predicted by the current model as a function of volume fraction where $\mu_f = 74.2$ GPa and $\mu_m = 1.02$ GPa.

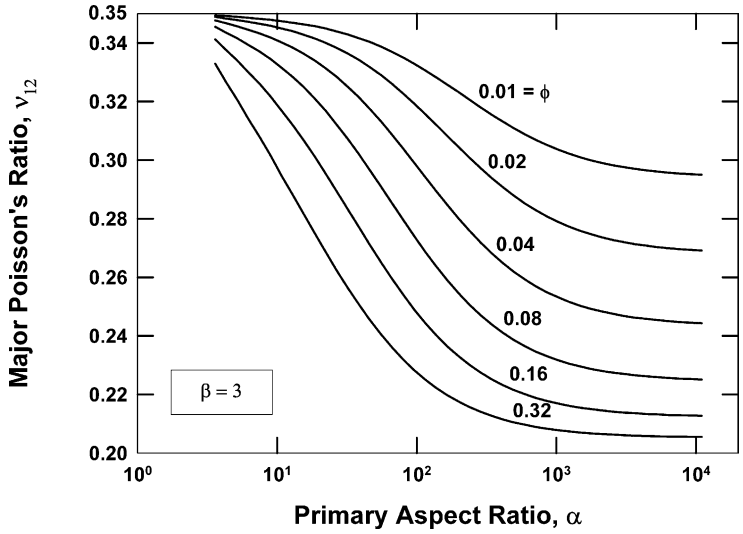

Fig. 20. Effects of the primary aspect ratio on the Poisson's ratio, ν_{12}, with secondary aspect ratio $\beta=3$ where Poisson's ratios of the matrix $\nu_m=0.35$ and the filler $\nu_f=0.2$.

$$J_{13} = \frac{\alpha^2(4\pi - \omega_1 - \omega_2)}{(\alpha^2 - 1)}$$

$$3J_{11} = 4\pi - J_{12} - J_{13}$$

$$J_{21} = \frac{(\omega_2 - 2\omega_1)}{(\beta^2 - 1)}$$

$$J_{23} = \frac{\alpha^2(4\pi - 2\omega_2 + \omega_1)}{(\alpha^2 - \beta^2)}$$

$$3J_{22} = 4\pi - J_{21} - J_{23}$$

$$J_{31} = \frac{(4\pi - \omega_1 - \omega_2)}{(\alpha^2 - 1)}$$

$$J_{32} = \frac{\beta^2(4\pi - 2\omega_2 + \omega_1)}{(\alpha^2 - \beta^2)}$$

$$3J_{33} = 4\pi - J_{31} - J_{32}$$

where α is the primary aspect ratio of the inclusion $= a_1/a_3$, and β is the secondary aspect ratio $= a_1/a_2$. The quantities a_1, a_2, and a_3 describe the dimensions of the ellipsoidal shape of the inclusions in the directions 1, 2, and 3, respectively. The parameters, ω_1 and ω_2 are given by

$$\omega_1 = \frac{4\pi\beta}{(\beta^2 - 1)(\alpha^2 - 1)^{1/2}}[F(K) - E(K)]$$

$$\omega_2 = 4\pi - \frac{4\pi\alpha^2}{(\alpha^2 - \beta^2)} + \frac{4\pi\alpha^2\beta E(K)}{(\alpha^2 - \beta^2)(\alpha^2 - 1)^{1/2}}$$

where $F(K)$ and $E(K)$ are the complete elliptical integrals of the first and the second kinds, respectively. Details are given in Appendix B.

When the primary aspect ratio of the inclusions is much larger than the secondary aspect ratio and much larger than 1, the above equations can be compactly expressed as follows

$$\omega_1 = \frac{4\pi\beta}{\alpha(\beta^2 - 1)}[F(K) - E(K)]$$

$$\omega_2 = \frac{4\pi\beta E(K)}{\alpha}$$

Appendix B. Elliptical integrals of the first and the second kinds

The elliptical integrals are well-known, and can be found in the WIKIPEDIA (The Free Encyclopedia) at internet site of http://en.wikipedia.org/.

B.1. Complete elliptical integral of the first kind

The elliptical integral of the first kind $F(\theta, K)$ is expressed as follows

$$F(\theta, K) = \int_0^\theta (1 - K^2\sin^2\phi)^{-1/2} d\phi$$

$$\theta = \sin^{-1}\left(1 - \frac{a_3^2}{a_1^2}\right)^{1/2}$$

$$K^2 = \frac{(a_1^2 - a_2^2)}{(a_1^2 - a_3^2)}$$

It is not easy to calculate $F(\theta, K)$ analytically, but this can be done numerically using Simpson's integral method. At $\theta = \pi/2$, $F(\theta, K)$ can be expressed as follows

$$F(K) = F\left(\frac{\pi}{2}, K\right) = \int_0^{\pi/2} (1 - K^2 \sin^2\phi)^{-1/2} \mathrm{d}\phi$$

When θ is $\pi/2$ and K^2 is almost 1 (i.e. $\alpha = \beta$), it can be calculated without error using the polynomial series equation

$$\begin{aligned} F(K) &= F\left(\frac{\pi}{2}, K\right) \\ &= \frac{\pi}{2}\left\{1 + \left(\frac{1}{2}\right)^2 K^2 + \left(\frac{1\times 3}{2\times 4}\right)^2 K^4 \right. \\ &\quad \left. + \left(\frac{1\times 3\times 5}{2\times 4\times 6}\right)^2 K^6 + \cdots\right\} \\ &= \frac{\pi}{2} \sum_{n=0}^{\infty} K^{2n} \frac{(2n)!(2n)!}{16^n n! n! n! n!} \end{aligned}$$

B.2. Complete elliptical integral of the second kind

The elliptical integral of second kind $E(\theta,K)$ means the perimeter of ellipsoid and can be expressed as follows

$$E(\theta, K) = \int_0^{\theta} (1 - K^2 \sin^2\phi)^{1/2} \mathrm{d}\phi$$

It is also calculated by Simpson's integral method.

$$E(K) = E\left(\frac{\pi}{2}, K\right) = \int_0^{\pi/2} (1 - K^2 \sin^2\phi)^{1/2} \mathrm{d}\phi$$

At $\theta = \pi/2$, $E(\theta,K)$ can also be simply calculated in terms of the polynomial series as follows

$$\begin{aligned} E(K) &= E\left(\frac{\pi}{2}, K\right) \\ &= \frac{\pi}{2}\left\{1 - \left(\frac{1}{2}\right)^2 K^2 - \left(\frac{1\times 3}{2\times 4}\right)^2 \frac{K^4}{3} \right. \\ &\quad \left. - \left(\frac{1\times 3\times 5}{2\times 4\times 6}\right)^2 \frac{K^6}{5} - \cdots\right\} \\ &= \frac{\pi}{2}\left\{1 - \sum_{n=1}^{\infty} \frac{K^{2n}}{(2n-1)} \frac{(2n)!(2n)!}{16^n n! n! n! n!}\right\} \end{aligned}$$

References

[1] Yoon PJ, Fornes TD, Paul DR. Polymer 2002;43(25):6727–41.
[2] Yalcin B, Cakmak M. Polymer 2004;45:6623–38.
[3] Eshelby JD. Proc R Soc London 1957;A241(1226):376–96.
[4] Hashin Z, Rosen BW. J Appl Mech 1964;31:223–32.
[5] Hill R. J Mech Phys Solids 1964;12:199–212.
[6] Halpin JC. Air Force Materials Laboratory, Technical Report 67-423; 1969.
[7] Chou TW, Nomura S, Taya M. J Compos Mater 1980;14(3):178–88.
[8] Russel WB. Appl Math Phys 1973;24:581–600.
[9] Mori T, Tanaka K. Acta Metall 1963;21:571–4.
[10] Benveniste Y. Mech Mater 1987;6:147–57.
[11] Mura T. Micromechanics of defects in solids. 2nd ed. The Hague: Martinus Nijhoff; 1987. p. 74.
[12] Tandon GP, Weng GJ. Polym Compos 1984;5:327–33.
[13] Fornes TD, Paul DR. Polymer 2003;44:4993–5013.
[14] Brune DA, Bicerano J. Polymer 2002;43:369–87.
[15] Tucker CL, Liang E. Compos Sci Technol 1999;59:655–71.
[16] Gibbson RF. Principles of composite material mechanics. New York: McGraw-Hill; 1994.
[17] Hill R. J Mech Phys Solids 1963;11:357–72.